Mechanisms of Carrier Transport Induced by a Microswimmer Bath

Andreas Kaiser*, Andrey Sokolov, Igor S. Aranson, and Hartmut Löwen

***Abstract*—It was shown that a wedgelike microparticle (referred to as "carrier") exhibits a directed translational motion along the wedge cusp if it is exposed to a bath of microswimmers. Here we model this effect in detail by resolving the microswimmers explicitly using interaction models with different degrees of mutual alignment. Using computer simulations we study the impact of these interactions on the transport efficiency of a V-shaped carrier. We show that the transport mechanism itself strongly depends on the degree of alignment embodied in the modeling of the individual swimmer dynamics. For weak alignment, optimal carrier transport occurs in the turbulent microswimmer state and is induced by swirl depletion inside the carrier. For strong aligning interactions, optimal transport occurs already in the dilute regime and is mediated by a polar cloud of swimmers in the carrier wake pushing the wedge-particle forward. We also demonstrate that the optimal shape of the carrier leading to maximal transport speed depends on the kind of interaction model used.**

***Index Terms*—Computational modeling, dynamics, micromotor, microorganisms, nanobioscience, physics.**

I. Introduction

THE collective properties of active fluids have been studied intensively in the last years [1]–[4]. Examples of such active matter can be found in a broad class of systems ranging from bacteria [5]–[8], alga [9]–[11], spermatozoa [12]–[14], animals [15]—like birds [16], fish [17], or insects [18], [19]—and even human beings [20]–[22]. All of these systems can be categorized as *living* active matter. Additionally, there is a broad class of *artificial* realizations, based on various propulsion mechanisms like pure body rotation [23], propulsion by attached flagella [24]–[26] or various chemically induced mechanisms like self-diffusiophoresis [27]–[32] or self-thermophoresis [33]–[35].

These swimmers are known to exhibit spatiotemporal active states like swarming [36]–[39] and turbulence (swirling) [40]–[48]. Most of these patterns can be obtained by a simple modeling based on the excluded volume effects of effective anisotropic objects [42], [49]. However, the actual particle collisions and the degree of alignment are supposed to play an important role [50], [51]. Mutual alignment of colliding swimmers provides a mechanism of swarming [52], as observed for many artificial active systems [51], [53]–[55]. On the other hand, experiments have shown a swim-off effect of two bacteria after the collisions [5], [56], [57].

In the last years, active fluids in the presence of passive objects and obstacles have been considered in experiments and simulations. Fixed boundaries have been shown to guide and accumulate active particles [58]–[64]. This effect has been used to rectify the motion of swimmers [65]–[69], and designing sorting [70]–[73] as well as trapping devices for microswimmers [59], [74], [75]. The motion of passive particles submersed in complex systems [76], like active fluids, has been studied as well. The study includes simple small spherical [77]–[79] and curved [80] tracer particles to large deformable chains [81], showing a regime of ballistic motion [29], [82], [83].

Recently, it has been shown that energy can be extracted from active fluids and biomolecular motors [84]. Asymmetric cogwheels, submersed in an active bath, spontaneously rotate [85]–[88]. Moreover, it has been demonstrated recently that wedgelike microparticles can be transported in the highly dilute [89] and in the turbulent state [90] of the active bath.

Here, we focus on the modeling of the dynamics of a wedgelike microparticle (referred to in the following as "carrier") when it is exposed to a bath of microswimmers. These V-shape particles can be fabricated by photolithography [35], [86], [91] and can be submersed into a bath of biological or artificial microswimmers. By using an external magnetic field, the carrier is only allowed to translate but not to rotate. In this paper, we resolve the microswimmers explicitly using different interaction models with various degrees of alignment after a binary collision. We study the impact of these interactions on the transport efficiency of the carrier in detail and show that the transport mechanisms itself strongly depends on the degree of alignment embodied in the modeling of the individual swimmer dynamics. In earlier work [90], the maximal carrier speed occurred in the turbulent state and caused by swirl depletion. Here we show that for strongly aligning interactions the picture is different: an even higher transport speed can be achieved in a dilute active fluid which is induced by a smectic ordered cluster in the wake of the carrier. In contrast to earlier work [89], here a full swarm has developed to push the carrier in an efficient way. We also optimize the shape of the carrier maximizing the transport speed and show that it depends on the kind of interaction model used.

Manuscript received August 08, 2014; revised September 25, 2014; accepted October 03, 2014. *Asterisk indicates corresponding author.*

The work of A. Kaiser was supported by the ERC Advanced Grant INTERCOCOS (Grant No. 267499). The work of H. Löwen was supported by the SPP 1726 of the DFG. The work of A. Sokolov and I. S. Aranson was supported by the U.S. Department of Energy (DOE), Office of Science, Basic Energy Sciences (BES), Materials Science and Engineering Division.

*A. Kaiser is with the Institut für Theoretische Physik II: Weiche Materie, Heinrich-Heine-Universität Düsseldorf, 40225 Düsseldorf, Germany (e-mail: kaiser@thphy.uni-duesseldorf.de).

A. Sokolov and I. S. Aranson are with the Materials Science Division, Argonne National Laboratory, Argonne, IL 60439 USA.

H. Löwen is with the Institut für Theoretische Physik II: Weiche Materie, Heinrich-Heine-Universität Düsseldorf, 40225 Düsseldorf, Germany.

Color versions of one or more of the figures in this paper are available online at http://ieeexplore.ieee.org.

Digital Object Identifier 10.1109/TNB.2014.2361652

This paper is organized as follows: Firstly, we specify our modeling in Section II. Secondly, we study and compare the collective behavior in Section III. In Section IV we study the transport efficiency of a wedgelike carrier and deduce the underlying mechanisms, which are directly linked to swimmer-swimmer interactions. Furthermore, we compute the optimal shape of the carrier which leads to the maximum transport speed. Finally, we conclude in Section V.

II. Model

We model the active bath in two spatial dimensions by considering N rodlike self-propelled particles with center-of-mass positions $\mathbf{r}_\alpha$ and orientations $\hat{\mathbf{u}}_\alpha$ $(\alpha = 1, \ldots, N)$, using a possible effective body shape asymmetry analogous to reference [90] in the absence of noise and hydrodynamic interactions. Hydrodynamic interactions between the swimmers are ignored which is justified at high packing in the absence of any global flow. Each rod of length ℓ and width λ is discretized into $n = 6$ spherical segments equidistantly positioned along the main rod axis $\hat{\mathbf{u}} = (\cos\varphi, \sin\varphi)$. The aspect ratio of the swimmers is fixed to $\ell/\lambda = 5$ according to a previous work regarding the explicit realization *Bacillus subtilis*. A repulsive Yukawa potential is imposed between the segments of different rods [92]. The resulting total pair potential of a rod pair α, β is given by $U_{\alpha\beta} = \sum_{i=1}^{n}\sum_{j=1}^{n} U_i U_j \exp[-r_{ij}^{\alpha\beta}/\lambda]/r_{ij}^{\alpha\beta}$ where λ is the screening length defining the particle diameter, and $r_{ij}^{\alpha\beta} = |\mathbf{r}_i^\alpha - \mathbf{r}_j^\beta|$ the distance between segment i of rod α and j of rod β $(\alpha \neq \beta)$. The effective body shape[1] of the rods can be tuned by the interaction prefactor of the first segment of each rod with respect to the others, see Fig. 1. This quantity will be given by the ratio $U^* = U_1^2/U_j^2$ $(j = 2 \ldots n)$, where $U^* = 1$ refers to a symmetric rod. Any overlap of particles is avoided by imposing a large interaction strength $U_j^2 = 2.5F_0\ell$. The shape asymmetry allows us to control the degree of alignment during a binary rod-rod collision [93]. Here we study *two situations* in detail: the symmetric case where $U^* = 1$, to realize an nematic alignment like in [38], [55], [94], and asymmetric rods, with $U^* = 3$, to mimic the swim-off effect observed for colliding bacteria, see Fig. 1(b). In the following, we refer to these two situations as models with weak or strong alignment. The self-propulsion is introduced by an effective self-propulsion force F_0 which is directed along the main rod axis leading to a constant propulsion velocity v_0 [95]. For anisotropic single particles it has been shown that this is an appropriate modeling of the coarse-grained propulsion mechanism [96], [97]. Although the swimmer is in principle force-free F_0 can be viewed as an effective force bringing the rods into motion. We do not resolve details of the actual propulsion mechanism.

Colloidal microswimmers move in the low Reynolds number regime, the corresponding overdamped equations of motion for the positions and orientations are

$$\mathbf{f}_\mathcal{T} \cdot \partial_t \mathbf{r}_\alpha(t) = -\nabla_{\mathbf{r}_\alpha} U(t) + F_0 \hat{\mathbf{u}}_\alpha(t), \tag{1}$$

$$\mathbf{f}_\mathcal{R} \cdot \partial_t \hat{\mathbf{u}}_\alpha(t) = -\nabla_{\hat{\mathbf{u}}_\alpha} U(t). \tag{2}$$

[1]The term *effective body shape* arises from the interaction landscape around a rod, e.g., by requesting that the interaction energy of a neighbouring segment is a thermal energy. This would result in an effective body shape.

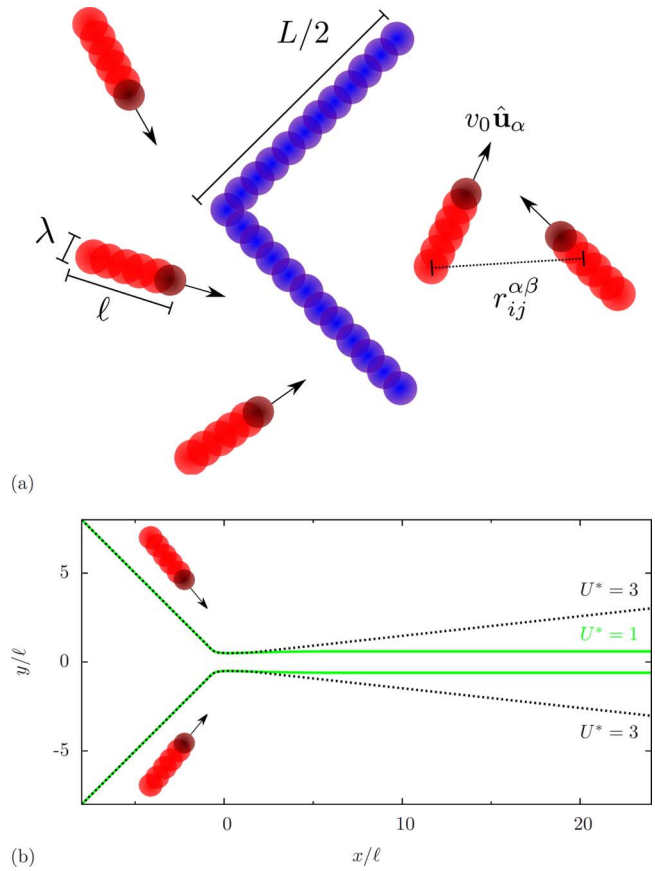

Fig. 1. (a) Sketch of the system of self-propelled rods with aspect ratio ℓ/λ and an effective self-propulsion velocity v_0 directed along the main rod axis $\hat{\mathbf{u}}$. The single six Yukawa segments are shown by red circles—a larger interaction prefactor for the first segment of each rod is indicated by darker color. A wedgelike carrier with a short contour length L is shown by blue circles. (b) Trajectories of colliding swimmers with varied interaction strengths.

Here the total potential energy is given by $U = (1/2)\sum_{\alpha,\beta(\alpha\neq\beta)} U_{\alpha\beta} + \sum_\alpha U_{\alpha<}$ with $U_{\alpha<}$ the potential energy of rod α with the carrier (the subscript $<$ is associated with the carrier). The one-body translational and rotational friction tensors for the rods $\mathbf{f}_\mathcal{T}$ and $\mathbf{f}_\mathcal{R}$ can be decomposed into parallel $f_\parallel$, perpendicular $f_\perp$, and rotational $f_\mathcal{R}$ contributions which depend solely on the aspect ratio $a = \ell/\lambda$ [98]

$$\frac{2\pi}{f_\parallel} = \ln a - 0.207 + 0.980a^{-1} - 0.133a^{-2}, \tag{3}$$

$$\frac{4\pi}{f_\perp} = \ln a + 0.839 + 0.185a^{-1} + 0.233a^{-2}, \tag{4}$$

$$\frac{\pi a^2}{3f_\mathcal{R}} = \ln a - 0.662 + 0.917a^{-1} - 0.050a^{-2}. \tag{5}$$

The resulting self-propulsion speed $v_0 = F_0/f_\parallel$ sets the characteristic time unit $\tau = \ell/v_0$. We ignore thermal fluctuations.

The friction coefficients in (3)–(5) apply to a single rod in an unbounded three-dimensional fluid. In two-dimensional systems there is an additional confinement induced by the presence of the carrier and by possible substrates on which the bacterial motion takes place. This would imply more complicated modeling of the friction tensors. However, our results actually do not depend sensitively on the ratio of the friction coefficients which justifies the relatively simple modeling assumed here.

According to previous experiments [90], the motion of the submersed carrier can be restricted to translation by using an external magnetic field which keeps the orientation of the carrier fixed. The carrier-swimmer interaction is implemented analogously to the swimmers by tiling the contour length L into Yukawa segments using an interaction strength $U_{jk}^2 = 2.5F_0\ell$ between the segments j of the rod and k of the carrier. Most of our data are obtained for $L = 26\ell$ but we do also vary the contour length L.

The resulting equation of motion for the carrier is

$$\mathbf{f}_< \cdot \partial_t \mathbf{r}_<(t) = -\nabla_{\mathbf{r}_<} \sum_\alpha U_{<\alpha}(t), \tag{6}$$

where $\mathbf{f}_<$ corresponds to the hydrodynamic friction tensor of the wedgelike carrier, calculated for the specific geometry of the carrier using the software package HYDRO++ [99], [100].

We use a square simulation box with area $A = (3L/\sqrt{2})^2$, ensuring that the domain is much larger than the carrier itself and periodic boundary conditions in both directions. The total number of swimmers is determined by $N = A\phi/\lambda\ell$, where ϕ is a dimensionless packing fraction.

III. Bulk Behavior

Here, we characterize the emergent dynamical states for both considered situations in absence of the carrier. As suitable order parameters we use the averaged swimming speed $\langle v_\alpha\rangle/v_0$, with $v_\alpha = \langle|\mathbf{r}_\alpha(t+\Delta t) - \mathbf{r}_\alpha(t)|\rangle/\Delta t$, the mean swimmer displacement during a time step $\Delta t = 10^{-3}\tau$, and the enstrophy $\Omega = 1/2\langle|[\nabla \times \mathbf{V}(\mathbf{r},t)]\cdot\hat{\mathbf{e}}_z|^2\rangle$ for a velocity field $\mathbf{V}(\mathbf{r},t)$ coarse-grained in space over three swimmer lengths. The results are shown in Figs. 2(a) and 2(b) and show qualitatively the same behavior for both situations, though the achieved values for $\langle v_\alpha\rangle/v_0$ and Ω are slightly higher for swimmers with less alignment. In agreement with experiments [42], [101], we can distinguish between three dynamical states as a function of increasing swimmer density. For low swimmer packing fractions, $\phi \lesssim 0.25$, the average swimmer velocity is $\langle v_\alpha\rangle \gtrsim 0.6v_0$ due to small amount of collisions, leading to a *dilute* state. For larger densities $0.25 \lesssim \phi \lesssim 0.75$ the velocity is almost constant and the system reveals a large enstrophy Ω for both systems. Since the enstrophy is a convenient indicator for bacterial turbulence [42], [49], we will refer to this state as *turbulent*. For high densities $0.75 \lesssim \phi$ the system becomes dynamically *jammed*, $\langle v_\alpha\rangle \lesssim 0.5v_0$. Using the equal-time spatial velocity autocorrelation function, we can determine the typical swirl radius R for various swimmer concentrations by its first minimum [49]. Hereby, in case of the asymmetric particle model, the typical swirls size is larger, see Fig. 2(c).

To quantify the influence of the body shape asymmetry on the (collective) motion of the swimmers, we study the alignment of the coarse-grained velocity field and the similarly coarse-grained orientation field $\mathbf{U}(\mathbf{r},t)$ using the coefficient C

$$C = \frac{\langle\cos\theta\rangle - \frac{2}{\pi}}{1 - \frac{2}{\pi}}, \tag{7}$$

where θ is the angle between both fields, see Fig. 2(d). Perfectly parallel fields lead to $C = 1$, while random directions reveal $C = 0$, hence $\langle\cos\theta\rangle = 2/\pi$ for $\theta \in \{-\pi/2, \pi/2\}$. In case of the symmetric rods, the mutual collisions in the dilute regime already form dense aligned clusters, leading to high alignment of the two fields. With increasing swimmer densities and the emergence of large scaled swirls the coefficient C decreases. As is intuitively expected, stronger alignment interaction leads to larger alignment between the two fields.

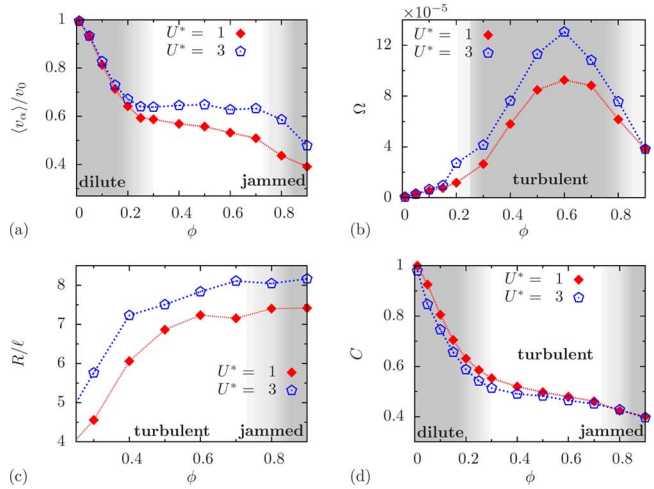

Fig. 2. Comparison of different bulk quantities for system with weak (open symbols) and strong (filled symbols) alignment. (a) Averaged reduced swimmer velocity $\langle v_\alpha\rangle/v_0$, (b) mean vorticity Ω, (c) typical reduced swirl size R/ℓ, and (d) alignment coefficient C as a function of swimmer packing fraction. Shaded areas indicate the emergent dynamical states.

IV. Transport of a Wedgelike Carrier

A. Transport Efficiency

Now, we study the transport efficiency v/v_0 of a wedgelike carrier for both alignment situations. Due to the symmetry of the wedge any averaged directed motion perpendicular to the apex will vanish.[2] In the apex direction there is no such symmetry and due to rectification the carrier will propagate along this direction. The resulting transport efficiency v/v_0 is shown in Fig. 3 for two selected contour lengths of the carrier.

While the maximal transport efficiency in around 0.25 for the asymmetric particles, as confirmed by experiment [90], the efficiency for symmetric swimmer is larger $v/v_0 \approx 0.35$. Moreover, the characteristic density for which the transport is optimal is vastly different: it occurs at low densities in the dilute regime for strong alignment but is significantly shifted towards the turbulent regime for weak alignment. However, both aliment conditions reveal an almost constant efficiency in the turbulent regime. Finally, if the active fluids jam, the carrier velocity clearly decreases as well.

B. Optimization of Wedge Shape

Here, we focus on the carrier geometry leading to maximal transport efficiency. Firstly, we choose the density which showed the highest transport and vary the apex angle for a fixed contour length $L = 26\ell$, see Fig. 4(a). Clearly, there has to be an optimal angle between zero and 180 degrees as these two extreme cases do not lead to any transport at all. As a result,

[2]For other types of locomotion, e.g., droplets driven by the Marangoni effect, an isotropic state can lead to directed motion, due to the instability of the stationary state at high Péclet numbers. This is, however, not the case in the system considered here.

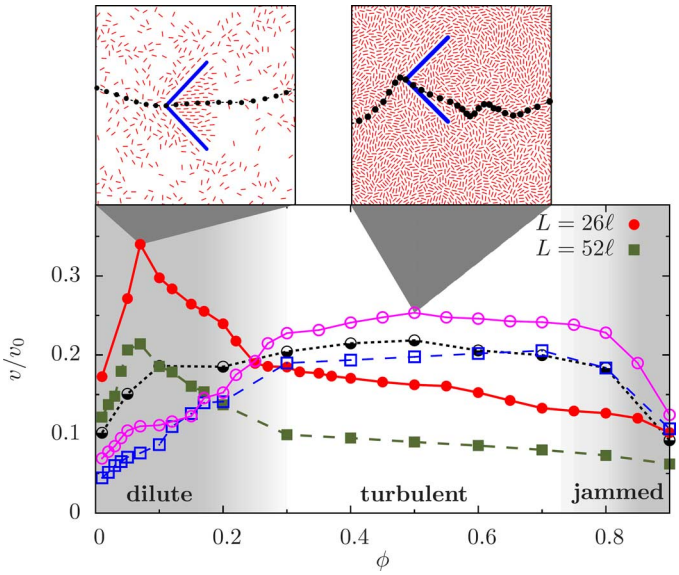

Fig. 3. Transport efficiency for various swimmer densities and two contour lengths of the carrier, $L = 26\ell$ (circles) and $L = 52\ell$ (squares). Filled symbols correspond to strong, open ones to weak alignment and half-filled ones to an intermediate alignment, estabilshed by $U^* = 2$. The dynamical states are indicated by shaded areas. The insets show the temporal progress of the carrier position indicated by the dotted line.

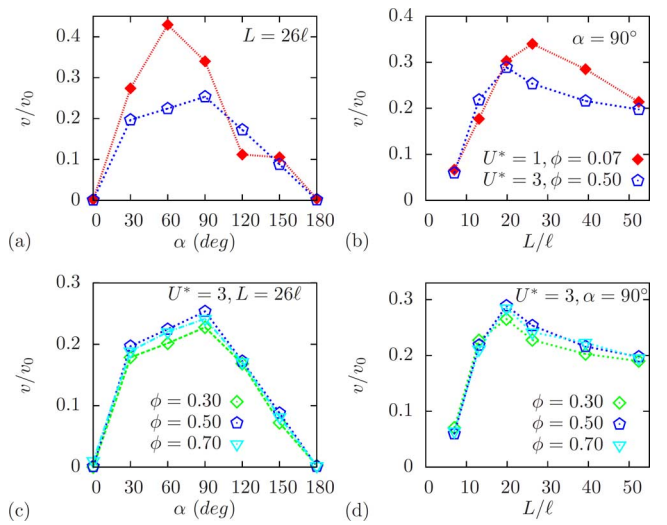

Fig. 4. Transport speed for (a) varied apex angle and fixed contour length $L = 26\ell$ and (b) varied length and fixed apex angle $\alpha = 90°$ for both situations at a fixed given swimmer packing fraction ϕ. Efficiency for varied packing fraction ϕ for the strong alignment model in the case of (c) varied apex angle and (d) carrier length.

the optimal wedge for weak alignment has an apex angle $\alpha = 90°$ while the optimal angle in the strong alignment model is around $\alpha = 60°$. In contrast to the weak alignment the transport efficiency is decreased drastically for apex angles $\alpha > 90°$.

Secondly, we have modified the length for a given apex angle $\alpha = 90°$, see Fig. 4(b). As before, let us start with the consideration of the two extreme cases. $L/\ell \to 0$ should not lead to any directed transport, while for $L/\ell \to \infty$ only a minor one is expected. We find an optimal length of $L \approx 20\ell$ in the weak alignment model and a larger length of $L \approx 26\ell$ in the strong alignment model. The optimal carrier length and apex angle do not depend strongly on the packing fraction in the turbulent regime, see Figs. 4(c) and 4(d)

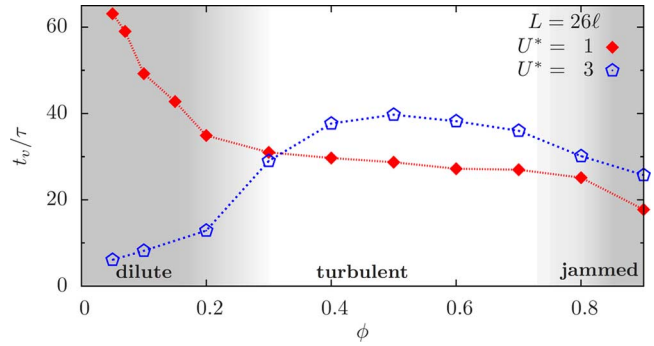

Fig. 5. Velocity correlation time t_v/τ for both particle models, a carrier with contour length $L = 26\ell$ and varied swimmer packing fraction.

C. *Transport Mechanism*

We recapitulate the transport mechanisms for the weak alignment model which has been recently explained by swirl shielding inside the carrier [90]. When turbulence sets in, a shielding of turbulent fluctuation near the walls of the carrier emerges. Due to the wedgelike geometry this shielding is more pronounced inside the carrier than outside. Thus a shielded area near the cusp emerges. Swimmers are trapped inside this area for a long time and thereby transport the wedge since they are rectified by the carrier. This process is limited by the flipping processes of the pushing microswimmers inside the wedge. The latter gives rise to fluctuations in the carrier velocity which are characterized by a typical correlation time scale t_v. This time t_v is set by the decay of the normalized and shifted carrier velocity autocorrelation function defined as

$$C_v(t) = \frac{\langle v(t_0)v(t_0+t)\rangle - \langle v\rangle^2}{\langle v^2\rangle - \langle v\rangle^2}. \tag{8}$$

A numerical fit reveals that this quantity decays as $\exp(-t/t_v)$ from which the typical correlation time t_v can be extracted. The results are plotted in Fig. 5 for the two alignment situations considered in this work. There is no such swirl shielded area outside the wedge as the swirls can sweep all swimmers away. This imbalance pushes the carrier forward. Clearly, this mechanism is valid for both alignment situations in the turbulent state. The achieved transport efficiency (see Fig. 3) is larger for weak alignment since the typical swirl size is larger than in the strong alignment case (see again Fig. 2) and therefore the corresponding swirl-shielded area is larger leaving more space for pushing microswimmers. As a consequence of the swirl shielding concept, the optimal transport is achieved when the apex width of the carrier is comparable to the typical swirl size, $L = 2\sqrt{2}R \approx 21\ell$, see again Fig. 4.

For strong alignment interactions, the swirl-shielding concept is overwhelmed by another mechanism which occurs already in the dilute regime. Fig. 6 shows the local density and the swimmer orientation (by plotting the average $\langle\cos\varphi\rangle$ around the carrier) for both alignment cases. The density exhibits a "hot spot" near the cusp and a depleted zone in the wake of the carrier. Due to the directed transport the carrier acts like a *bulldozer* and accumulates swimmers in its front. The intensity plot for the swimmer orientation shows a clear rectification of swimmers within the wedge even in the wake, where a large smectic cluster is formed, see left inset of Fig. 3. This cluster can only

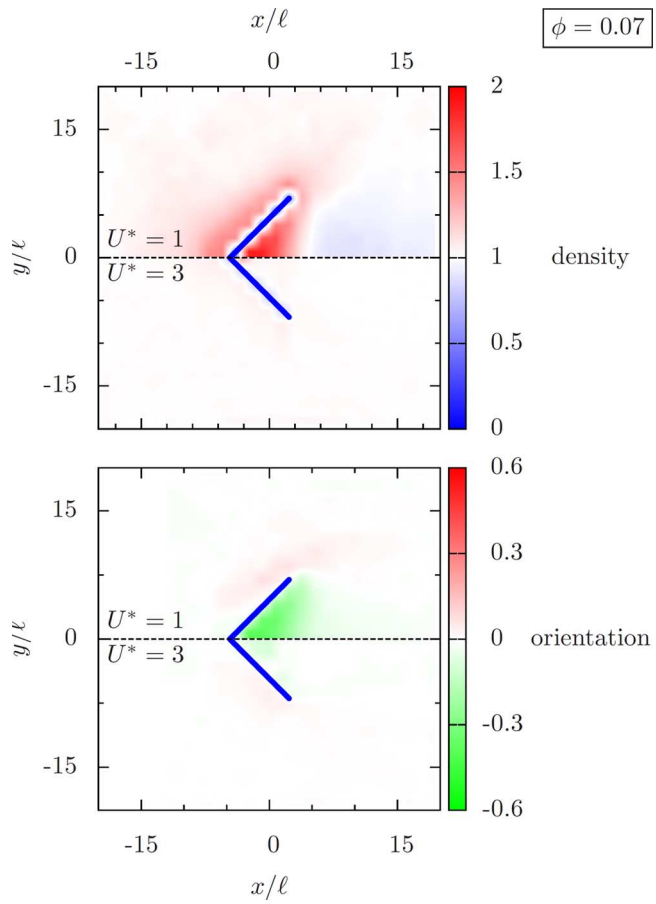

Fig. 6. Intensity plots for (top) the local swimmer density around the carrier and (bottom) the averaged swimmer orientations, using $\langle \cos \varphi \rangle$ for the situation of both alignments and a packing fraction $\phi = 0.07$.

emerge for sufficiently small apex angles, which explains the observed decay of transport efficiency for increasing apex angles, see again Fig. 4(a). This cluster is very stable as indicated by a large correlation time t_v in the carrier velocity, see again Fig. 5, leading to persistent straight motion of the carrier.

To supplement this picture, we present the data for the local average density in front of the carrier (ϕ_f) and in its wake (ϕ_w) in Fig. 7. The emergent smectic cluster in the wake of the carrier for the strong alignment model leads to $\phi_f/\phi_w \to 0$ for small swimmer densities, see Fig. 7(a) which supports the strong transport efficiency. When collective motion emerges in the bulk, the ratio ϕ_f/ϕ_w becomes larger than unity implying that the transport efficiency is decreased. For the weak alignment model this ratio is always larger than unity, see Fig. 7(b). This can be confirmed by experiments on *Bacillus subtilis* and a microwedge with a contour length $L = 52\ell$ [90], see Fig. 7(c). We predict this ratio by a simple scaling argument in the dilute regime. The carrier velocity is $v \sim v_0\phi$ and the achieved directed motion leads to a density gradient [$v \sim D\nabla\phi$, with $D \sim v_0\ell/\phi_w$]. According to this, we can approximate the resulting density ratio for a moving carrier by $\phi_f/\phi_w - 1 \sim \phi$, which is shown in the inset of Fig. 7(b).

To summarize, there are two different mechanisms at work for optimal carrier transport, namely swirl shielding for weak aligning interactions and a large polar pushing cloud of swimmers for strong alignment interactions. The first occurs in the

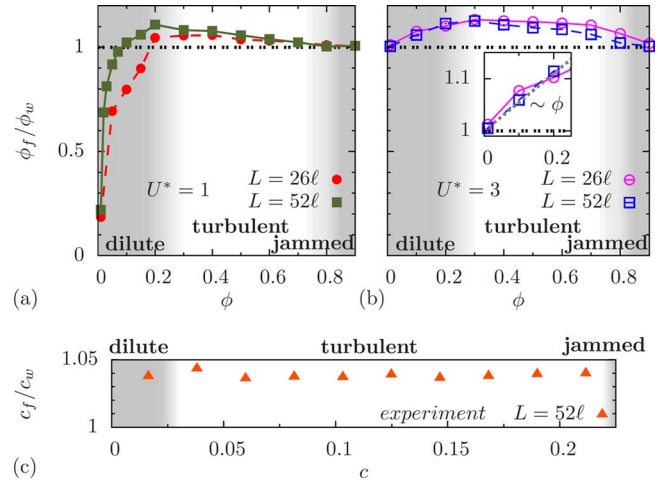

Fig. 7. Comparison of the density around the carrier using the ratio ϕ_f/ϕ_w, i.e., the ratio of the two densities in the front and in the wake for both interaction models, the two selected contour lengths as before and varied swimmer packing fractions ϕ. The inset in (b) shows a close up for the dilute state and a linear dependence of the ratio on the packing fraction ϕ. (c) Experimentally obtained concentration ratio c_f/c_w, with c the three-dimensional volume fraction.

turbulent regime while the latter is in the dilute regime. Finally, additional simulations reveal that there is a gradual crossover between these regimes and not a sharp jump as U^* is increased from 1 to 3.

V. Conclusion

We have demonstrated that the actual transport speed of a passive microwedge ("carrier") immersed into an active bath depends on the aligning properties of the individual microswimmers. For strong aligning interactions, as realized for artificial rod-like microswimmers, a polar oriented cloud in the wake of the carrier pushes the carrier forward. Conversely, for interaction without strong alignment, as realized for bacterial swimmers, the most efficient transport occurs in the turbulent state of the active bath and is caused by swirl depletion. Our results were obtained by computer simulations and can be verified in experiments. In particular, experiment with artificial microswimmers exhibiting a strong aligning interaction are highly desirably to test the predicted picture of a polar-ordered wake.

Future studies should investigate in more detail the hydrodynamic interactions between the particles in confinement following the recent work of Lushi *et al.* [48]. One also should focus on different shapes of carriers like L-particles or C-particles which have been considered theoretically [80], [93] but should be realized in experiments. Finally, the carrier transport can be possibly used as building block to fabricate more complicated micro- and nanomachines steered by an active bath.

Acknowledgment

The authors would like to thank Borge ten Hagen for helpful discussion.

References

[1] P. Romanczuk, M. Bär, W. Ebeling, B. Linder, and L. Schimansky-Geier, "Active Brownian particles: From individual to collective stochastic dynamics," *Eur. Phys. J. Spec. Top.*, vol. 202, pp. 1–162, 2012.

[2] M. E. Cates, "Diffusive transport without detailed balance in motile bacteria: Does microbiology need statistical physics?," *Rep. Prog. Phys.*, vol. 75, 2012, No. 042601.

[3] M. C. Marchetti, J. F. Joanny, S. Ramaswamy, T. B. Liverpool, J. Prost, M. Rao, and R. A. Simha, "Hydrodynamics of soft active matter," *Rev. Mod. Phys.*, vol. 85, pp. 1143–1189, 2013.

[4] I. S. Aranson, "Active colloids," *Physics-Uspekhi*, vol. 56, pp. 79–92, 2013.

[5] A. Sokolov, I. S. Aranson, J. O. Kessler, and R. E. Goldstein, "Concentration dependence of the collective dynamics of swimming bacteria," *Phys. Rev. Lett.*, vol. 98, 2007, No. 158102.

[6] V. B. Shenoy, D. T. Tambe, A. Prasad, and J. A. Theriot, "A kinematic description of the trajectories of *Listeria monocytogenes* propelled by actin comet tails," *Proc. Natl. Acad. Sci. USA*, vol. 104, p. 8229, 2007.

[7] S. Schmidt, J. ven der Gucht, P. M. Biesheuvel, R. Weinkamer, E. Helfer, and A. Frey, "Non-Gaussian curvature distribution of actin-propelled biomimetic colloid trajectoriess," *Eur. Biophys. J.*, vol. 37, pp. 1361–1366, 2008.

[8] J. Schwarz-Linek, C. Valeriani, A. Cacciuto, M. E. Cates, D. Marenduzzo, A. N. Morozov, and W. C. K. Poon, "Phase separation and rotor self-assembly in active particle suspensions," *Proc. Natl. Acad. Sci. USA*, vol. 109, pp. 4052–4057, 2012.

[9] M. Polin, I. Tuval, K. Drescher, J. P. Gollub, and R. E. Goldstein, "Chlamydomonas swims with two 'gears' in a eukaryotic version of run-and-tumble locomotion," *Science*, vol. 325, pp. 487–490, 2009.

[10] J. S. Guasto, K. A. Johnson, and J. P. Gollub, "Oscillatory flows induced by microorganisms swimming in two dimensions," *Phys. Rev. Lett.*, vol. 105, 2010, No. 168102.

[11] R. Ma, G. S. Klindt, I. H. Riedel-Kruse, F. Jülicher, and B. M. Friedrich, "Active phase and amplitude fluctuations of flagellar beating," *Phys. Rev. Lett.*, vol. 113, 2014, No. 048101.

[12] I. H. Riedel, K. Kruse, and J. Howard, "A self-organized vortex array of hydrodynamically entrained sperm cells," *Science*, vol. 309, pp. 300–303, 2005.

[13] B. M. Friedrich and F. Jülicher, "The stochastic dance of circling sperm cells: Sperm chemotaxis in the plane," *New J. Phys.*, vol. 10, 2008, No. 123035.

[14] D. M. Woolley, "Motility of spermatozoa at surfaces," *Reproduction*, vol. 216, pp. 259–270, 2003.

[15] T. Vicsek and A. Zafeiris, "Collective motion," *Phys. Rep.*, vol. 517, pp. 71–140, 2012.

[16] M. Ballerini, N. Cabibbo, R. Candelier, A. Cavagna, E. Cisbani, I. Giardina, V. Lecomte, A. Orlandi, G. Parisi, A. Procaccini, M. Viale, and V. Zdravkovic, "Interaction ruling animal collective behavior depends on topological rather than metric distance: Evidence from a field study," *Proc. Natl. Acad. Sci. USA*, vol. 105, pp. 1232–1237, 2008.

[17] Y. Katz, K. Tunstrøm, C. C. Ioannou, C. Huepe, and I. D. Couzin, "Inferring the structure and dynamics of interactions in schooling fish," *Proc. Natl. Acad. Sci. USA*, vol. 108, pp. 18720–18725, 2011.

[18] J. Buhl, D. J. T. Sumpter, I. D. Couzin, J. J. Hale, E. Despland, E. R. Miller, and S. J. Simpson, "From disorder to order in marching locusts," *Science*, vol. 312, pp. 1402–1406, 2006.

[19] A. John, A. Schadschneider, D. Chowdhury, and K. Nishinari, "Trafficlike collective movement of ants on trails: Absence of a jammed phase," *Phys. Rev. Lett.*, vol. 102, 2009, No. 108001.

[20] J. Zhang, W. Klingsch, A. Schadschneider, and A. Seyfried, "Ordering in bidirectional pedestrian flows and its influence on the fundamental diagram," *J. Stat. Mech. Theory Experiment*, vol. 2012, p. 02002, 2012.

[21] D. Helbing, I. Farkas, and T. Vicsek, "Simulating dynamical features of escape panic," *Nature*, vol. 407, pp. 487–490, 2000.

[22] J. L. Silverberg, M. Bierbaum, J. P. Sethna, and I. Cohen, "Collective motion of humans in mosh and circle pits at heavy metal concerts," *Phys. Rev. Lett.*, vol. 110 , 2013, No. 228701.

[23] A. Ghosh and P. Fischer, "Controlled propulsion of artificial magnetic nanostructured propellers," *Nano Lett.*, vol. 9, pp. 2243–2245, 2009.

[24] R. Dreyfus, J. Baudry, M. L. Roper, M. Fermigier, H. A. Stone, and J. Bibette, "Microscopic artificial swimmers," *Nature*, vol. 437, p. 862, 2005.

[25] P. Tierno, R. Golestanian, I. Pagonabarraga, and F. F. Sagues, "Magnetically actuated colloidal microswimmers," *J. Phys. Chem. B*, vol. 112, pp. 16525–16528, 2008.

[26] I. S. M. Khalil, H. C. Dijkslag, L. Abelmann, and S. Misra, "MagnetoSperm: A microrobot that navigates using weak magnetic fields," *Appl. Phys. Lett.*, vol. 104, 2014, No. 223701.

[27] W. F. Paxton, K. C. Kistler, C. C. Olmeda, A. Sen, S. K. S. Angelo, Y. Cao, T. E. Mallouk, P. E. Lammert, and V. H. Crespi, "Catalytic nanomotors: Autonomous movement of striped nanorods," *J. Amer. Chem. Soc.*, vol. 126, pp. 13424–13431, 2004.

[28] S. Fournier-Bidoz, A. C. Arsenault, I. Manners, and G. A. Ozin, "Synthetic self-propelled nanorotors," *Chem. Commun.*, vol. 441, pp. 441–443, 2005.

[29] J. R. Howse, R. A. L. Jones, A. J. Ryan, T. Gough, R. Vafabakhsh, and R. Golestanian, "Self-motile colloidal particles: From directed propulsion to random walk," *Phys. Rev. Lett.*, vol. 99, 2007, No. 048102.

[30] J. Palacci, C. Cottin-Bizonne, C. Ybert, and L. Bocquet, "Sedimentation and effective temperature of active colloidal suspensions," *Phys. Rev. Lett.*, vol. 105, 2010, No. 088304.

[31] R. Kapral, "Perspective: Nanomotors without moving parts that propel themselves in solution," *J. Chem. Phys.*, vol. 138, 2013, No. 020901.

[32] S. Sanchez, A. A. Solovev, S. M. Harazim, and O. G. Schmidt, "Microbots swimming in the flowing streams of microfluidic channels," *J. Amer. Chem. Soc.*, vol. 133, pp. 701–703, 2011.

[33] H.-R. Jiang, N. Yoshinaga, and M. Sano, "Active motion of a Janus particle by self-thermophoresis in a defocused laser beam," *Phys. Rev. Lett.*, vol. 105, 2010, No. 268302.

[34] G. Volpe, I. Buttinoni, D. Vogt, H.-J. Kümmerer, and C. Bechinger, "Microswimmers in patterned environments," *Soft Matter*, vol. 7, pp. 8810–8815, 2011.

[35] F. Kümmel, B. ten Hagen, R. Wittkowski, I. Buttinoni, R. Eichhorn, G. Volpe, H. Löwen, and C. Bechinger, "Circular motion of asymmetric self-propelling particles," *Phys. Rev. Lett.*, vol. 110, 2013, No. 198302.

[36] S. Thutupalli, R. Seemann, and S. Herminghaus, "Swarming behavior of simple model squirmers," *New J. Phys.*, vol. 13, 2011, No. 073021.

[37] Y. Yang, V. Marceau, and G. Gompper, "Swarm behavior of self-propelled rods and swimming flagella," *Phys. Rev. E*, vol. 82, 2010, No. 031904.

[38] F. Ginelli, F. Peruani, M. Bär, and H. Chaté, "Large-scale collective properties of self-propelled rods," *Phys. Rev. Lett.*, vol. 104, 2010, No. 184502.

[39] X. Chen, X. Dong, A. Be'er, H. L. Swinney, and H. P. Zhang, "Scale-invariant correlations in dynamic bacterial clusters," *Phys. Rev. Lett.*, vol. 108, 2012, No. 148101.

[40] A. Sokolov and I. S. Aranson, "Physical properties of collective motion in suspensions of bacteria," *Phys. Rev. Lett.*, vol. 109, 2012, No. 248109.

[41] D. Saintillan and M. J. Shelley, "Instabilities, pattern formation, and mixing in active suspensions," *Phys. Fluids*, vol. 20, 2008, No. 123304.

[42] H. H. Wensink, J. Dunkel, S. Heidenreich, K. Drescher, R. E. Goldstein, H. Löwen, and J. M. Yeomans, "Meso-scale turbulence in living fluids," *Proc. Natl. Acad. Sci. USA*, vol. 109, pp. 14308–14313, 2012.

[43] K.-A. Liu and I. Lin, "Bacterial turbulence reduction by passive magnetic particle chains," *Phys. Rev. E*, vol. 88, 2013, No. 033004.

[44] I. Aranson, "The aquatic dance of bacteria," *Physics*, vol. 6, p. 61, 2013.

[45] M. Abkenar, K. Marx, T. Auth, and G. Gompper, "Collective behavior of penetrable self-propelled rods in two dimensions," *Phys. Rev. E*, vol. 88, 2013, No. 062314.

[46] A. Rabani, G. Ariel, and A. Be'er, "Collective motion of spherical bacteria," *PLoS ONE*, vol. 8, 2013, No. E83760.

[47] S. Zhou, A. Sokolov, O. D. Lavrentovich, and I. S. Aranson, "Living liquid crystals," *Proc. Natl. Acad. Sci. USA*, vol. 111, pp. 1265–1270, 2014.

[48] E. Lushi, H. Wioland, and R. E. Goldstein, "Fluid flows created by swimming bacteria drive self-organization in confined suspensions," *Proc. Natl. Acad. Sci. USA*, vol. 111, pp. 9733–9738, 2014.

[49] H. H. Wensink and H. Löwen, "Emergent states in dense systems of active rods: from swarming to turbulence," *J. Phys. Condens. Matter*, vol. 24, 2012, No. 464130.

[50] A. Bricard, J.-B. Caussin, N. Desreumaux, O. Dauchot, and D. Bartolo, "Emergence of macroscopic directed motion in populations of motile colloids," *Nature*, vol. 503, pp. 95–98, 2013.

[51] E. Ferrante, A. E. Turgut, M. Dorigo, and C. Huepe, "Elasticity-based mechanism for the collective motion of self-propelled particles with springlike interactions: A model system for natural and artificial swarms," *Phys. Rev. Lett.*, vol. 111, 2013, No. 268302.

[52] T. Vicsek, A. Czirók, E. Ben-Jacob, I. Cohen, and O. Shochet, "Novel type of phase transition in a system of self-driven particles," *Phys. Rev. Lett.*, vol. 75, pp. 1226–1229, 1995.

[53] A. Kudrolli, G. Lumay, D. Volfson, and L. S. Tsimring, "Swarming and swirling in self-propelled polar granular rods," *Phys. Rev. Lett.*, vol. 100, 2008, No. 058001.

[54] V. Narayan, S. Ramaswamy, and N. Menon, "Long-lived giant number fluctuations in a swarming granular nematic," *Science*, vol. 317, pp. 105–108, 2007.

[55] W. Wang, W. Duan, A. Sen, and T. E. Mallouk, "Catalytically powered dynamic assembly of rod-shaped nanomotors and passive tracer particles," *Proc. Natl. Acad. Sci. USA*, vol. 110, pp. 17744–17749, 2013.

[56] I. S. Aranson, A. Sokolov, J. O. Kessler, and R. E. Goldstein, "Model for dynamical coherence in thin films of self-propelled microorganisms," *Phys. Rev. E*, vol. 75, 2007, No. 040901.

[57] K. Drescher, J. Dunkel, L. H. Cisneros, S. Ganguly, and R. E. Goldstein, "Fluid dynamics and noise in bacterial cell–cell and cell–surface scattering," *Proc. Natl. Acad. Sci. USA*, vol. 108, pp. 10940–10945, 2011.

[58] P. Denissenko, V. Kantsler, D. J. Smith, and J. Kirkman-Brown, "Human spermatozoa migration in microchannels reveals boundary-following navigation," *Proc. Natl. Acad. Sci. USA*, vol. 109, pp. 8007–8010, 2012.

[59] A. Guidobaldi, Y. Jeyaram, I. Berdakin, V. V. Moshchalkov, C. A. Condat, V. I. Marconi, L. Giojalas, and A. V. Silhanek, "Geometrical guidance and trapping transition of human sperm cells," *Phys. Rev. E*, vol. 89, 2014, No. 032720.

[60] H. H. Wensink and H. Löwen, "Aggregation of self-propelled colloidal rods near confining walls," *Phys. Rev. E*, vol. 78, 2008, No. 031409.

[61] A. M. Menzel, "Unidirectional laning and migrating cluster crystals in confined self-propelled particle systems," *J. Phys. Condens. Matter*, vol. 25, 2013, No. 505103.

[62] C. F. Lee, "Active particles under confinement: aggregation at the wall and gradient formation inside a channel," *New J. Phys.*, vol. 15, 2013, No. 055007.

[63] J. Elgeti and G. Gompper, "Wall accumulation of self-propelled spheres," *Europhys. Lett.*, vol. 101, 2013, No. 48003.

[64] Y. Fily, A. Baskaran, and M. F. Hagan, "Dynamics of self-propelled particles under strong confinement," *Soft Matter*, vol. 10, pp. 5609–5617, 2014.

[65] M. B. Wan, C. J. O. Reichhardt, Z. Nussinov, and C. Reichhardt, "Rectification of swimming bacteria and self-driven particle systems by arrays of asymmetric barriers," *Phys. Rev. Lett.*, vol. 101, 2008, No. 018102.

[66] J. Tailleur and M. E. Cates, "Sedimentation, trapping, and rectification of dilute bacteria," *Europhys. Lett.*, vol. 86, 2009, No. 60002.

[67] A. Pototsky, A. M. Hahn, and H. Stark, "Rectification of self-propelled particles by symmetric barriers," *Phys. Rev. E*, vol. 87, 2013, No. 042124.

[68] F. Q. Potiguar, G. A. Farias, and W. P. Ferreira, "Self-propelled particle transport in regular arrays of rigid asymmetric obstacles," *Phys. Rev. E*, vol. 90, 2014, No. 012307.

[69] P. Galajda, J. Keymer, P. Chaikin, and R. Austin, "A wall of funnels concentrates swimming bacteria," *J. Bacteriol.*, vol. 189, pp. 8704–8707, 2007.

[70] S. E. Hulme, W. R. DiLuzio, S. S. Shevkoplyas, L. Turner, M. Mayer, H. C. Berg, and G. M. Whitesides, "Using ratchets and sorters to fractionale motile celles of *Escherichia coli* by length," *Lab Chip*, vol. 8, pp. 1888–1895, 2008.

[71] J. A. Drocco, C. J. O. Reichhardt, and C. Reichhardt, "Bidirectional sorting of flocking particles in the presence of asymmetric barriers," *Phys. Rev. E*, vol. 85, 2012, No. 056102.

[72] I. Berdakin, Y. Jeyaram, V. V. Moshchalkov, L. Venken, S. Dierckx, S. J. Vanderleyden, A. V. Silhanek, C. A. Condat, and V. I. Marconi, "Influence of swimming strategy on microorganism separation by asymmetric obstacles," *Phys. Rev. E*, vol. 87, 2013, No. 052702.

[73] A. Costanzo, J. Elgeti, T. Auth, G. Gompper, and M. Ripoll, "Motility-sorting of self-propelled particles in microchannels," *Europhys. Lett.*, vol. 107, 2014, No. 36003.

[74] A. Kaiser, H. H. Wensink, and H. Löwen, "How to capture active particles," *Phys. Rev. Lett.*, vol. 108, 2012, No. 268307.

[75] L. Restrepo-Pérez, L. Soler, C. S. Martínez-Cisneros, S. Sanchez, and O. G. Schmidt, "Trapping self-propelled micromotors with microfabricated chevron and heart-shaped chips," *Lab Chip*, vol. 14, pp. 1515–1518, 2014.

[76] A. Vagias, R. Raccis, K. Koynov, U. Jonas, H.-J. Butt, G. Fytas, P. Košovan, O. Lenz, and C. Holm, "Complex tracer diffusion dynamics in polymer solutions," *Phys. Rev. Lett.*, vol. 111, 2013, No. 088301.

[77] K. C. Leptos, J. S. Guasto, J. P. Gollub, A. I. Pesci, and R. E. Goldstein, "Dynamics of enhanced tracer diffusion in suspensions of swimming eukaryotic microorganisms," *Phys. Rev. Lett.*, vol. 103, 2009, No. 198103.

[78] G. Miño, J. Dunstan, A. Rousselet, E. Clement, and R. Soto, "Induced diffusion of tracers in a bacterial suspension: theory and experiments," *J. Fluid Mech.*, vol. 729, pp. 423–444, 2013.

[79] X.-L. Wu and A. Libchaber, "Particle diffusion in a quasi-two-dimensional bacterial bath," *Phys. Rev. Lett.*, vol. 84, pp. 3017–3020, 2000.

[80] S. A. Mallory, C. Valeriani, and A. Cacciuto, "Curvature indcued activation of a passive tracer in an active bath," *Phys. Rev. E*, vol. 90, 2014, No. 032309.

[81] A. Kaiser and H. Löwen, "Unusual swelling of a polymer in a bacterial bath," *J. Chem. Phys.*, vol. 141, 2014, No. 044903.

[82] B. ten Hagen, S. van Teeffelen, and H. Löwen, "Brownian motion of a self-propelled particle," *J. Phys. Condens. Matter*, vol. 23, 2011, No. 194119.

[83] X. Zheng, B. ten Hagen, A. Kaiser, M. Wu, H. Cui, Z. Silber-Li, and H. Löwen, "Non-Gaussian statistics for the motion of self-propelled Janus particles: Experiment versus theory," *Phys. Rev. E*, vol. 88, 2013, No. 032304.

[84] H. Hess, "Engineering applications of biomolecular motors," *Annu. Rev. Biomed. Eng.*, vol. 13, pp. 429–450, 2011.

[85] L. Angelani, R. DiLeonardo, and G. Ruocco, "Self-starting micromotors in a bacterial bath," *Phys. Rev. Lett.*, vol. 102, 2009, No. 048104.

[86] A. Sokolov, M. M. Apodaca, B. A. Grzyboski, and I. S. Aranson, "Swimming bacteria power microscopic gears," *Proc. Natl. Acad. Sci. USA*, vol. 107, pp. 969–974, 2010.

[87] R. DiLeonardo, L. Angelani, D. DellArciprete, G. Ruocco, V. Iebba, S. Schippa, M. P. Conte, F. Mecarini, F. D. Angelis, and E. D. Fabrizio, "Bacterial ratchet motors," *Proc. Natl. Acad. Sci. USA*, vol. 107, pp. 9541–9545, 2010.

[88] H. Li and H. P. Zhang, "Asymmetric gear rectifies random robot motion," *Europhys. Lett.*, vol. 102, 2013, No. 50007.

[89] L. Angelani and R. D. Leonardo, "Geometrically biased random walks in bacteria-driven micro-shuttles," *New J. Phys.*, vol. 12, 2010, No. 113017.

[90] A. Kaiser, A. Peshkov, A. Sokolov, B. ten Hagen, H. Löwen, and I. S. Aranson, "Transport powered by bacterial turbulence," *Phys. Rev. Lett.*, vol. 112, 2014, No. 158101.

[91] J. Gachelin, G. Miño, H. Berthet, A. Lindner, A. Rousselet, and E. Clément, "Non-Newtonian viscosity of *Escherichia coli* suspensions," *Phys. Rev. Lett.*, vol. 110, 2013, No. 268103.

[92] T. Kirchhoff, H. Löwen, and R. Klein, "Dynamical correlations in suspensions of charged rodlike macromolecules," *Phys. Rev. E*, vol. 53, pp. 5011–5022, 1996.

[93] H. H. Wensink, V. Kantsler, R. E. Goldstein, and J. Dunkel, "Controlling active self-assembly through broken particle-shape symmetry," *Phys. Rev. E*, vol. 89, 2014, No. 010302.

[94] S. Ramaswamy, "The mechanics and statistics of active matter," *Annu. Rev. Condens. Matter Phys.*, vol. 1, pp. 323–345, 2010.

[95] F. Kümmel, B. ten Hagen, R. Wittkowski, D. Takagi, I. Buttinoni, R. Eichhorn, G. Volpe, H. Löwen, and C. Bechinger, "Reply: Circular motion of asymmetric self-propelling particles," *Phys. Rev. Lett.*, vol. 113, 2014, No. 029802.

[96] B. ten Hagen, F. Kümmel, D. Takagi, H. Löwen, and C. Bechinger, "Gravitaxis of asymmetric self-propelled colloidal particles," *Nat. Commun.*, vol. 5, 2014, No. 4829.

[97] B. ten Hagen, R. Wittkowski, D. Takagi, F. Kümmel, C. Bechinger, and H. Löwen, "Can the self-propulsion of anisotropic microswimmers be described by using forces and torques?," *arXiv:1410.6707*, 2014.

[98] M. M. Tirado, C. L. Martinez, and J. Garcia de la Torre, "Comparison of theories for the translational and rotational diffusion-coefficients of rod-like macromolecules—Application to short DNA fragments," *J. Chem. Phys.*, vol. 81, pp. 2047–2052, 1984.

[99] J. Garcia de la Torre, S. Navarro, M. C. Lopez Martinez, F. G. Diaz, and J. J. L. Cascales, "HYDRO: A computer program for the prediction of hydrodynamic properties of macromolecules," *Biophys. J.*, vol. 67, pp. 530–531, 1994.

[100] B. Carrasco and J. Garcia de la Torre, "Improved hydrodynamic interaction in macromolecular bead models," *J. Chem. Phys.*, vol. 111, pp. 4817–4826, 1999.

[101] A. Sokolov and I. S. Aranson, "Reduction of viscosity in suspension of swimming bacteria," *Phys. Rev. Lett.*, vol. 103, 2009, No. 148101.